

A role for direct interactions in the modulation of rhodopsin by ω -3 polyunsaturated lipids

Alan Grossfield*, Scott E. Feller[†], and Michael C. Pitman**[‡]

*T. J. Watson Research Center, IBM, 1101 Kitchawan Road, Yorktown Heights, NY 10598; and [†]Department of Chemistry, Wabash College, 301 West Wabash Avenue, Crawfordsville, IN 47933

Edited by Barry H. Honig, Columbia University, New York, NY, and approved January 24, 2006 (received for review September 23, 2005)

Rhodopsin, the G protein-coupled receptor primarily responsible for sensing light, is found in an environment rich in polyunsaturated lipid chains and cholesterol. Biophysical experiments have shown that lipid unsaturation and cholesterol both have significant effects on rhodopsin's stability and function; ω -3 polyunsaturated chains, such as docosahexaenoic acid (DHA), destabilize rhodopsin and enhance the kinetics of the photocycle, whereas cholesterol has the opposite effect. Here, we use molecular dynamics simulations to investigate the possibility that polyunsaturated chains modulate rhodopsin stability and kinetics via specific direct interactions. By analyzing the results of 26 independent 100-ns simulations of dark-adapted rhodopsin, we found that DHA routinely forms tight associations with the protein in a small number of specific locations qualitatively different from the non-specific interactions made by saturated chains and cholesterol. Furthermore, the presence of tightly packed DHA molecules tends to weaken the interhelical packing. These results are consistent with recent NMR work, which proposes that rhodopsin binds DHA, and they suggest a molecular rationale for DHA's effects on rhodopsin stability and kinetics.

cholesterol | molecular dynamics | fatty acid | protein–lipid interactions

Rhodopsin, the primary light receptor in the visual system, is an integral membrane protein belonging to the G protein-coupled receptor (GPCR) superfamily. GPCRs, the largest known protein superfamily, are critically important in a wide variety of biological signaling processes (1). As a result, half of all current drug targets belong to this family (2). Moreover, rhodopsin is the only GPCR whose structure is known to atomic resolution (3–7), making it important both in its own right and as a template for understanding GPCR function in general (1, 8).

Rhodopsin is found in the rod outer-disk membranes in the photoreceptor cells of vertebrates and invertebrates (9). These membranes are highly enriched in ω -3 polyunsaturated fatty acids (10, 11); the cholesterol content is very high in newly formed disk membranes and drops as they mature (12). The presence of lipids with polyunsaturated chains destabilizes the native state of rhodopsin and speeds the kinetics of the photocycle (13, 14), whereas cholesterol stabilizes rhodopsin and slows its kinetics (13–15). Although these experiments deepen our understanding, the molecular-level details of how the membrane environment modulates rhodopsin's structure and function are unknown.

Molecular dynamics simulations can be a powerful tool to advance our understanding of protein–lipid biophysics. In recent years, a number of groups have published simulations of rhodopsin in monounsaturated (16–19) and polyunsaturated membranes (20, 21). Recent work from our group focused on the interactions between polyunsaturated lipids, cholesterol, and rhodopsin (20). In that work, we observed two docosahexaenoic acid (DHA) chains forming contacts deep in the protein interior, suggesting that DHA's effects on rhodopsin could possibly be explained by direct protein–lipid interactions, in addition to its effects on bulk properties (22, 23). If DHA binding occurs frequently and disrupts native contacts, it could readily explain

the decreased stability that occurs when rhodopsin is placed in a DHA-rich environment. This destabilization could then explain the enhanced photocycle kinetics, because the photocycle involves large-scale rigid body motions, which will break interhelical contacts (24, 25). However, in the original simulation, there were only two such events to different regions on the protein, making it difficult to assess their statistical significance.

In support of our previous results, we present a series of 26 independently constructed 100-ns simulations of rhodopsin [Protein Data Bank ID code 1U19 (3, 26)] in a membrane composed of a 2:2:1 mixture of 1-stearoyl-2-docosahexaenoyl-phosphatidylethanolamine, 1-stearoyl-2-docosahexaenoyl-phosphatidylcholine, and cholesterol. The results indicate that (i) tight DHA–rhodopsin association occurs fairly frequently on the hundred nanosecond time scale; (ii) these associations tend to take place at a small number of well defined regions on the protein; (iii) the presence of tightly packed DHAs in a specific region frequently leads to weakened interhelical residue–residue packing in that region; and (iv) whereas cholesterol and saturated chains sometimes pack tightly against the protein, their binding appears nonspecific relative to DHA.

Results

Bulk Chain Packing. Our primary tool for quantitating the tightness of packing between two molecules (e.g., a DHA chain and the protein) is the packing score, which we define to be the sum over all intermolecular atom pairs of $1/r^6$ (see *Methods* for details). We computed probability distributions of the packing scores of DHA, stearic acid (STEA), and cholesterol to characterize their interactions with rhodopsin; the results are plotted in Fig. 1. The majority of lipids have very low packing scores, which is to be expected because the packing score is a sum over a very short-ranged function ($1/r^6$). On a per-molecule basis, cholesterol is most likely to pack well against the protein, followed by DHA, then STEA. The lipid chains have smooth, relatively featureless probability distributions, whereas cholesterol has a pronounced minimum packing score of ≈ 0.15 . The error bars, defined as the standard deviation of the probability distributions from the 26 independent trajectories, show that, although our data clearly show that DHA is more likely to pack well relative to STEA, this result may not reliably emerge from a single 100-ns simulation. Indeed, in at least one of our simulations, the overall packing of STEA was tighter than DHA. The point is even clearer when we consider cholesterol; because there are far fewer cholesterol molecules in the system, the error bars are significantly larger, indicating that rhodopsin–cholesterol interactions vary widely across independent simulations.

Fig. 1B shows the same data rescaled according to membrane composition to produce the relative probability for the protein

Conflict of interest statement: No conflicts declared.

This paper was submitted directly (Track II) to the PNAS office.

Abbreviations: DHA, docosahexaenoic acid; STEA, stearic acid.

[†]To whom correspondence should be addressed. E-mail: pitman@us.ibm.com.

© 2006 by The National Academy of Sciences of the USA

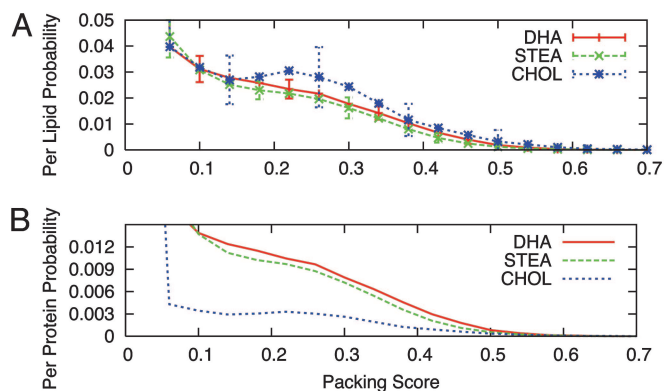


Fig. 1. Packing scores for membrane components. (A) The normalized probability distributions for the packing scores of DHA, STEA, and cholesterol. The error bars are the SD of the averages computed for the 26 independent trajectories and, as such, represent the uncertainty for the probability computed with a 100-ns simulation. Approximately 70% of the lipids have packing scores between 0 and 0.1. (B) The relative probability for the protein to make a given packing score with each membrane component, computed by taking the data from A and rescaling according to the relative abundance of DHA, STEA, and cholesterol molecules in the system.

to make a given packing score with each membrane component. Fig. 1A shows the probability distribution for a given lipid, whereas Fig. 1B shows the relative likelihood for the protein to make a specific packing score with each lipid type, taking composition into account. As a result, Fig. 1B shows that the majority of tightly packed membrane components are lipid chains rather than cholesterol.

By contrast, Fig. 2 answers a somewhat different question: Of the chains that pack tightly, how many are DHA vs. STEA? Fig. 2 clearly shows that the majority of the tightly packed chains are DHA, whereas STEA chains are more likely to interact weakly. This finding is as expected, given previous simulations showing that lipids with a saturated and polyunsaturated chain preferentially orient the polyunsaturated chain toward rhodopsin (20, 27). These results are also consistent with recent NMR work showing that lipids containing polyunsaturated chains preferentially concentrate at the surface of rhodopsin (28).

Localization of Tightly Packed Lipids. Although component preferences are already apparent from the above probability distributions, it is interesting to ask whether there are specific regions on the protein that are more likely to associate with different lipid species. For example, recent NMR experiments have suggested that rhodopsin contains a number of DHA binding sites (28). Although the present simulations cannot directly comment on the thermodynamics of lipid binding to rhodopsin, it is reasonable to suggest that regions on the protein that tend to pack tightly with lipid chains may correspond to binding sites.

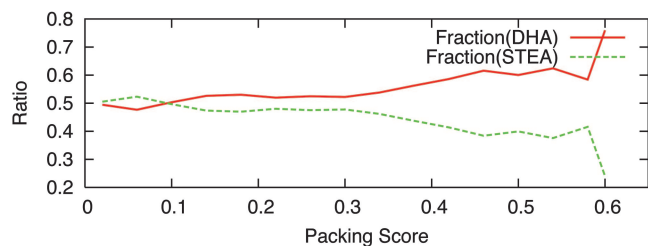


Fig. 2. Fraction of lipid chains with a given score, summed over all lipids in all trajectories. Scores of >0.6 are merged into a single bin to improve statistics.

Table 1. Groups of residues which preferentially interact with tight-packing DHA chains

Group	Frequency	Residues	Helices
1	10	266, 269, 270, 273, 274, 277, 278	6
2	14	36, 39, 286, 290	1, 7
3	9	129, 130, 133, 148, 152, 155, 156, 159	3, 4
4	4	45, 48, 92, 95, 96, 99	1, 2
5	9	256, 301, 304, 305, 308, 309	6, 7
6	4	50, 300, 304, 307, 308, 314	1, 7
7	7	133, 136, 137, 142, 143, 146, 148	3, 4
8	5	252, 255, 256, 259	6
Ungrouped	16		
Total	78	43	

The residues listed are those that have packing score $S > 0.05$ in the normalized average profile for their group. Frequency indicates the number of lipids that interacted with this group of residues, and the helices shown indicate which secondary structure elements contain those residues. The totals indicate the total number of lipids considered and the number of unique residues selected in the groups.

Accordingly, we examined the degree to which lipid-chain binding is localized on the protein surface by computing the packing score between a given chain and each residue in the protein; we refer to the resulting 348-dimensional vector as the packing profile (see *Methods* for details; see also *Supporting Methods*, which is published as supporting information on the PNAS web site). We computed packing profiles for the tightest-packed DHA, STEA, and cholesterol chains and performed a cluster analysis on these profiles (see *Methods* for details). We then examined the average profiles for the resulting groups and identified the residues that made significant protein-lipid contacts.

Tables 1–3 show the results of this analysis. Several interesting points can be gleaned immediately from the data. First, there are more well defined clusters for DHA than for STEA and cholesterol. Moreover, $\approx 80\%$ of the DHAs examined fell into a well defined group, whereas only 32% of STEAs and 24% of cholesterol fell in significant clusters. These data indicate that DHA binding occurs in a relatively small number of well defined ways and that STEA and cholesterol packing, although occasionally just as tight, is largely nonspecific.

Second, there are some locations on the protein that appear to generally favor tight lipid packing without specifically favoring a particular lipid species. For example, DHA groups 5 and 6, STEA group 2, and cholesterol group 2 are quite similar, indicating that the region between helices 6 and 7 encourages strong, well localized, lipid-independent packing. Similarly, STEA group 1 and cholesterol group 3 contain the same strongly interacting residues, which indicates a preference for more rigid, saturated lipids. By contrast, the other DHA groups appear to form regions specific to DHA.

Third, localized tight packing typically occurs between helices, rather than along a single helix (Tables 1–3 and Fig. 3). The most interesting exception is STEA group 3 and to some extent STEA

Table 2. Groups of residues which preferentially interact with tight-packing STEA chains

Group	Frequency	Residues	Helices
1	4	108, 111, 112, 115, 172	3, 4
2	5	256, 300, 301, 304, 305, 308, 309	6, 7
3	4	217, 220, 221, 224, 225, 228	5
4	4	205, 208, 209, 213, 273	4, 5
Ungrouped	36		
Total	53	23	

See Table 1 for details.

Table 3. Groups of residues that preferentially interact with tight-packing cholesterol molecules

Group	Frequency	Residues	Helices
1	4	53, 56, 57, 60, 320, 321	1, 8
2	5	252, 255, 256, 259, 260, 305, 308, 309	6, 7
3	6	108, 111, 112, 115, 172	3, 4
Ungrouped	47		
Total	62	19	

See Table 1 for details.

group 4; the residues in question line the outside of helix 5, away from any other contacts with the protein. Note that tight packing is not restricted to the highlighted regions; these are merely the regions where tight packing was reproducible and well characterized. In fact, the single tightest binding event for DHA, similar to one of the two binding events in our original simulation (20), occurred only once in the present ensemble of 26 simulations and, thus, is not represented in Fig. 3. Rather, the present group analysis assumes that the simulations are sufficiently representative of the equilibrium ensemble that the most important binding motifs occur frequently.

Fig. 4 is an attempt to answer a slightly different question: Do specific regions of the protein interact preferentially with one membrane component, or is tight packing determined solely by protein geometry, independent of local membrane composition? For example, in the parts of the protein where the groups from Tables 1–3 overlap, is there one particular membrane component that is most likely to bind? To answer these questions, we computed the packing score for each residue in the protein against all DHAs, STEAs, and cholesterols in all systems. We then selected the residues that had a statistically significant preference for one component. The results were projected onto the rhodopsin structure (Fig. 4). Fig. 4 confirms that the overlapping groups between helices 6 and 7 are largely nonspecific; most of the residues in that region have no significant

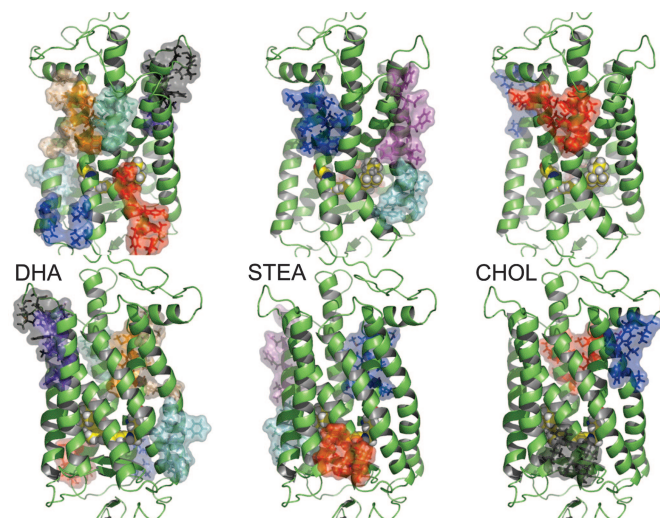


Fig. 3. Groups of residues that tightly associate with membrane components, projected onto the 1U19 crystal structure. *Upper* and *Lower* are views with helices 6 and 4 in front, respectively. (*Left*) The residues that interact with DHA are highlighted. (*Center*) The residues that interact with STEAs are highlighted. (*Right*) The residues that interact with cholesterol are highlighted. Different colors indicate the distinct groups defined in Tables 1–3. The “binding sites” for different membrane components overlap in places, most notably between helices 6 and 7 (upper left part of the protein) (*Upper*) and between helices 3 and 4 (bottom center of the protein) (*Lower*).

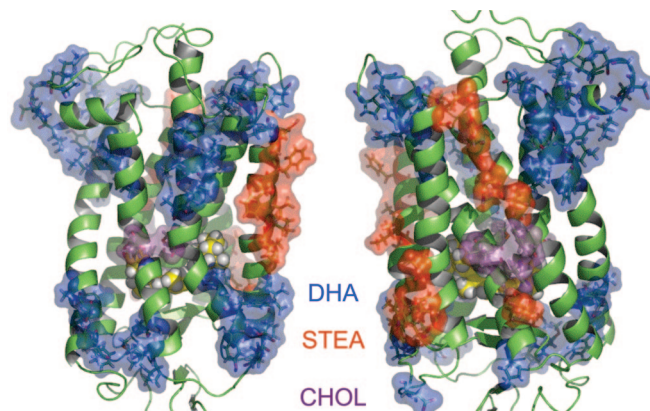


Fig. 4. Groups of residues that preferentially interact with DHA, STEA, or cholesterol projected onto the 1U19 crystal structure. The average packing score between each residue and each membrane component was computed across all simulations. Residues are colored blue if the DHA score is significantly higher than that for STEA and cholesterol. Residues for which the STEA score is significantly higher are shown in red. Magenta residues have significantly higher cholesterol scores. Green residues have either no significant preference or very weak overall signals. In all cases, significance was determined by comparing the difference between the two values with the sum of the standard errors in those values.

preference for DHA, STEA, or cholesterol. Overall, many more residues have a preference for DHA (51 residues) than STEA (16 residues) or cholesterol (5 residues), including all of residues in the protein core that have a significant preference. It is also interesting to note that the residues that prefer cholesterol are located in a narrow belt near the center of the membrane.

Discussion

There has been a strong interest in the biological importance of polyunsaturated lipids for many years. DHA in particular has been implicated in a variety of conditions, including neurological and developmental problems (29), heart disease (30), autoimmune disorders (31–33), and psychological problems (34–36). Membranes rich in DHA have low-order parameters, higher compressibility, and other interesting physical characteristics (22, 37). An interesting question is whether these bulk properties are solely responsible for DHA’s biological effects (37, 38) or whether direct protein–lipid interactions are involved (20, 28).

The present work is an attempt to connect these ideas via molecular dynamics simulations. Using a large number of long, independently constructed trajectories, we found evidence for regions on rhodopsin that tightly associate with lipid chains, especially DHA (see Fig. 3). Although we cannot assess the thermodynamic importance of these observations in any quantitative way, it is suggestive that rhodopsin packs with DHA in a far more localized manner than with STEA or cholesterol. In other words, tight DHA–protein packing largely occurs in a small number of regions in well characterized ways, whereas STEA and cholesterol packing is relatively nonspecific, with a much larger number of weakly populated associations. This qualitative difference is consistent with experimental evidence for DHA binding but not STEA binding (28).

The identification of several tightly associating regions specific for DHA suggests a previously uncharacterized mechanism for DHA’s effects on rhodopsin stability and kinetics: DHA’s penetration of the protein core may displace native interactions, destabilizing the native state and facilitating the transition to the active form. Fig. 3 and Table 1 clearly show that DHA chains tend to pack tightly in well defined regions, primarily grooves between helices. Because the stability of the native state rests in part on interhelix sidechain–sidechain interactions, the sugges-

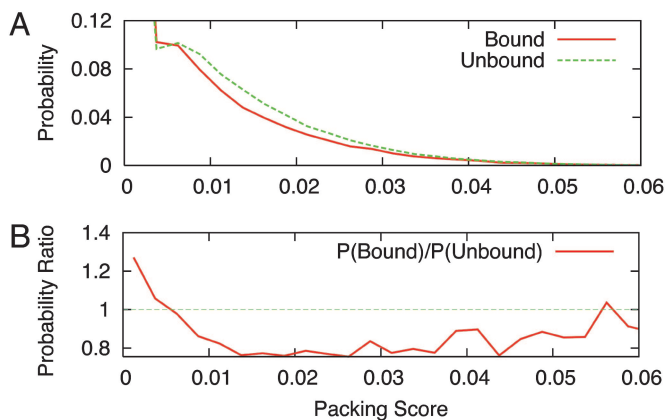


Fig. 5. Comparison of residue–residue packing scores from trajectories with and without lipids bound to those sites. We computed normalized histograms for the packing scores for interhelix residue pairs found in the groups from Table 1 (see text for details). (A) The probability distributions. (B) Ratio of the probability distributions.

tion that DHA intercalation into these regions must be disruptive seems straightforward. Although we cannot directly assess the effect of DHA binding on protein thermodynamic stability, we can compare the packing quality for residues in the binding groups in simulations during which there was a binding event to the same quantity in simulations during which no binding occurred. Specifically, we considered the following residue pairs: from group 2 (Table 2), N36–I286 and M39–I290; from group 3, V130–G156 and V130–F159; from group 4, F45–L95 and I48–T92; from group 5, R252–M309 and I256–I305; from group 6, L50–V300; and from group 7, Y136–P142, V137–F146, I133–F148, and V137–M143. We computed the packing scores for each of these residue pairs from all trajectories and separated the ones that had a binding event at their respective groups from the rest. Thus, when examining residues F45–L95 and I48–T92 from group 4, there were four trajectories that contributed to the “bound” category and 22 that contributed to the “unbound” category. We then computed the probability distributions for all bound and unbound residue pairs. Fig. 5 shows the results, which clearly indicate that the presence of bound lipids weakens interhelical packing. Fig. 5A shows that the probability of a high residue–residue packing score is significantly reduced when DHAs are present in the packing groups. The means for the bound and unbound distributions (0.0079 and 0.0096, respectively) differ significantly; the probability that this difference would arise randomly is $<10^{-5}$ according to the Student *t* test, even assuming that the data has a coherence time of 10 ns, which is very conservative. The difference is more dramatically shown in Fig. 5B, which shows the ratio of the probability distribution functions: upon binding, the probability of very low packing scores is enriched by $\approx 25\%$, whereas the probability of tighter packing is significantly depleted, indicating that some native contacts are being broken and that the interhelical residues are generally more loosely packed.

However, the presence of tight-packing DHAs did not weaken all of the interhelical residue packings. DHA binding at groups 2, 4, and 6 (from Table 1) is correlated with weaker interhelical packing, whereas binding at groups 3 and 5 seemed to tighten packing. For group 7, the behavior is more complicated; the packing between Y136–P142 and V137–F146 got weaker, and the packing between I133–F148 and V137–M143 got stronger. Examining the structure of rhodopsin shows that these residues are in helices 3 and 4 and their connecting loop and that these changes in packing indicate that there are

significantly different loop structures in the lipid-binding trajectories compared with the unbound trajectories.

Cholesterol has an ordering effect on bulk membranes (16), and experiments (15, 39) and simulations (20) have suggested that its stabilization of rhodopsin is due to these bulk effects, rather than any direct interaction. The present simulations are consistent with this interpretation. Although the tightest packings in our simulations were between rhodopsin and cholesterol, they are relatively rare despite the cholesterol-rich membrane composition (Fig. 1B). Moreover, the binding events do not appear to favor specific residues significantly (Table 3 and Fig. 3), with $>75\%$ of the tightly packed cholesterols not falling into any well defined cluster.

Previous simulation work was able to discern an overall preference for DHA to congregate at the protein surface (20, 21). However, those works focused solely on the radial distribution of DHA, effectively averaging out axial variations. This approach was necessary, because the residence time for lipids at the protein surface was comparable with the simulation time scales, limiting statistical confidence. Indeed, the same would be true for any one of the simulations in the present work; the significance of the binding motifs emerges only from considering the ensemble of simulations. In any given 100-ns trajectory, only a small fraction of the packing sites are populated, and it is only by assessing the totality of the simulations that a pattern can be observed. Thus, although the individual simulations equilibrate rapidly [the states sampled are appropriate for the NVE (constant number, volume, and energy) ensemble at 311 K], 100 ns is not long enough for sampling to become ergodic. Examination of the time series for the packing score between individual lipids and the protein indicate that tight packing events tend to be long-lived on the simulation time scale, lasting many tens of nanoseconds. The presence of three distinct molecular species in the bilayer further complicates matters, because 100 ns is not long enough for large-scale lateral reorganization of the membrane, although we did see numerous examples of lipids entering and leaving the first “solvation shell” around the protein. Although in principle the same sampling could be achieved with a single long calculation, indirect evidence from our simulations suggests that such a simulation would have to be extremely long and, therefore, far less efficient than the present approach.

One caveat is, in a sense, the inverse of the problem we seek to solve: We don’t know what, if any, lateral organization might be present in our system. Our membrane construction protocol explicitly assumes that both lipid types should be randomly distributed; if there is a preference for one headgroup to segregate at the protein surface or at particular locations on the surface, our simulations would not necessarily capture that phenomenon. The same is true to an even greater extent when considering the cholesterols, because there are fewer of them in the system. The 10-ns axial correlation time suggested by previous simulations indicates that there is sufficient time for local exploration (27), but if the global distribution differs significantly from random distribution, the present simulations would likely underestimate it. The trends that emerge here should therefore be regarded as lower bounds. Still, the present approach represents a significant step forward from previous attempts, because it is very difficult to assess convergence from a single trajectory, no matter how long.

Conclusions

We present the results of molecular dynamics simulations of rhodopsin in a complex membrane environment rich in the ω -3 fatty acid DHA. By performing a large number of lengthy, independently constructed simulations, we were able to identify a number of well localized regions on rhodopsin, where DHA repeatedly packs tightly. We suggest that these packing regions may be related to recent experimental evidence for the existence of several specific rhodopsin–DHA binding sites (28). Because

the putative binding sites primarily involve grooves between helices and binding weakens interhelical packing, their existence suggests a role for direct lipid–protein interaction in DHA’s modulation of rhodopsin stability, kinetics, and function. By contrast, STEA and cholesterol packing appeared largely non-specific. Characterization of specific DHA-binding motifs was made possible only by combining a large number of lengthy, independent simulations; the independent starting conformations were necessary to explore distinct membrane configurations, whereas the 100-ns trajectories allowed sufficient time for local sampling.

Methods

Simulation Details. We performed 26 independent, 100-ns simulations of rhodopsin in an explicit membrane and water environment embedded in a periodic box. The lipid composition was chosen to be similar to that found biologically and in many model–membrane experiments (12–14, 40, 41). Long-range electrostatics were modeled by using the Ewald method, and real-space electrostatics and van der Waal’s interactions were smoothly truncated at 10 Å. The simulation was run in the NVE ensemble with an average temperature of 311 K. The CHARMM27 force field was used to represent the protein (42), and the recently refined CHARMM saturated chain (43), polyunsaturated chain (44), and cholesterol parameters (27) were used to describe the lipids. Construction and equilibration were performed with CHARMM 2.7 (45), and production calculations were performed with BLUE MATTER (46), a molecular dynamics package specially written to take advantage of the Blue Gene/L hardware (47). Production trajectories were run on 512, 1,024, or 2,048 Blue Gene nodes, yielding 4, 6, or 9 ns per day, respectively. In each case, the initial coordinates for the lipid and cholesterol were regenerated such that the simulations are truly independent. Each simulation was run for at least 100 ns, with the first 20 ns of each simulation excluded from analysis as equilibration. Total simulation time was more than 2.6 μ s. For further details, see *Supporting Methods*.

Membrane Construction. The membrane construction protocol was based on the strategy used by Woolf and Roux (48). We built the protein and internal water molecules by using the highest-resolution crystal structure for rhodopsin [Protein Data Bank ID code 1U19 (3, 26)]. Lipid and cholesterol conformations were chosen from a library generated by a 20-ns molecular dynamics simulation of a neat bilayer with the same composition as the one used here. Initial headgroup placements were chosen by relaxing the locations of spheres randomly placed at the appropriate distance from the membrane centers, and lipid coordinates were gradually relaxed in a manner that guaranteed minimal clashes with the protein and cholesterol. For further details, see *Supporting Methods*.

Packing Scores and Profiles. The packing score for a pair of molecules (e.g., rhodopsin and a DHA chain) was computed as a sum over atom pairs:

$$S = \sum_i^{\text{Protein}} \sum_j^{\text{Lipid}} \frac{1}{r_{ij}^6}. \quad [1]$$

This quantity is analogous to the attractive component of the Lennard–Jones potential and is related to the rate of magnetization transfer measured in recent NMR experiments (49). All atoms of both molecules were used.

The packing profile for each individual lipid chain was created by computing the average packing score between the chain and each individual residue in the protein, resulting in a vector with 348 components. Each profile was then normalized, removing information about the overall magnitude of the packing score (see *Supporting Methods* for further details). We perform this normalization to remove information about the duration of each packing event; because such packings are relatively long-lived on the simulation time scale, our measured lifetimes are largely determined by when the packing formed, which is not a physically significant quantity. Similarity between the profiles for two different lipids was estimated by using the dot product between the normalized profiles. We established the significance of different dot product values by using a form of Monte-Carlo bootstrapping, determining that the dot product distribution for random vectors is described by a Gaussian, with mean of 0.638 and SD of 0.034.

To further quantitate the different modes of tight packing, we clustered the packing profiles. Specifically, we selected the individual lipid components (DHA, STEA, and cholesterol) that had the highest maximum packing scores with the protein and compared their packing profiles. Any two profiles with a dot product of ≥ 0.75 (more than three SDs above the randomly expected value) were defined to be part of the same group. Groups with three or fewer members were not analyzed further, nor were groups for which the average pairwise dot product was not significantly greater than what would be expected for a random collection of unit vectors. As a result, the clustering procedure produced groups which were well defined and distinct. The details of the process for selecting tightly packed chains and performing the clustering are contained in *Supporting Methods*.

To cleanly define the residues in the resulting groups, we examined the normalized average group profiles and selected those residues that had a renormalized score of 0.05 or greater to best represent the residues involved in the group’s binding events. However, none of the conclusions are particularly sensitive to this choice of threshold value. Although we do occasionally refer to these groups of residues as “binding sites,” we do not mean to imply that our data show these packings to be thermodynamically stable. Rather, we intend to indicate that these clusters cover the regions most frequently and reproducibly involved in the tightest associations in our simulations, which might be related to the binding sites suggested by recent NMR work (28).

We thank the members of the Blue Matter team (B. Fitch, R. Germain, A. Rayshubskiy, T. J. C. Ward, M. Eleftheriou, F. Suits, Y. Zhestkov, R. Zhou, J. Pitera, and W. Swope) for contributions and Frank Suits for help developing the tools used to perform the analysis. S.E.F. thanks the National Science Foundation for support through Award MCB-0091508 and the Dreyfus Foundation for support under the Henry Dreyfus Teacher–Scholar Program.

- Gether, U. (2000) *Endocr. Rev.* **21**, 90–113.
- Madabushi, S., Gross, A. K., Philippi, A., Meng, E. C., Wensel, T. G. & Lichtarge, O. (2004) *J. Biol. Chem.* **279**, 8126–8132.
- Okada, T., Sugihara, M., Bondar, A. N., Elstner, M., Entel, P. & Buss, V. (2004) *J. Mol. Biol.* **342**, 571–583.
- Palczewski, K., Kumasaka, T., Hori, T., Behnke, C. A., Motoshima, H., Fox, B. J., Le Trong, I., Teller, D. C., Okada, T., Stenkamp, R. E., *et al.* (2000) *Science* **289**, 739–745.
- Okada, T., Fujiyoshi, Y., Silow, M., Navarro, J., Landau, E. M. & Shichida, Y. (2002) *Proc. Natl. Acad. Sci. USA* **99**, 5982–5987.
- Li, J., Edwards, P. C., Burghammer, M., Villa, C. & Schertler, G. F. X. (2004) *J. Mol. Biol.* **343**, 1409–1438.
- Edwards, P. C., Li, J., Burghammer, M., McDowell, J. H., Villa, C., Hargrave, P. A. & Schertler, G. F. X. (2004) *J. Mol. Biol.* **343**, 1439–1450.
- Fanelli, F. & De Benedetti, P. G. (2005) *Chem. Rev.* **105**, 3297–3351.
- Yeagle, P. L. (2005) in *The Structure of Biological Membranes*, ed. Yeagle, P. L. (CRC, Boca Raton, FL), pp. 479–498.
- Stone, W. L., Farnsworth, C. C. & Dratz, E. A. (1979) *Exp. Eye Res.* **28**, 387–397.
- Boesze-Battaglia, K. & Albert, A. D. (1989) *Exp. Eye Res.* **49**, 699–701.
- Boesze-Battaglia, K., Hennessey, T. & Albert, A. D. (1989) *J. Biol. Chem.* **264**, 8151–8155.
- Mitchell, D. C., Niu, S.-L. & Litman, B. J. (2001) *J. Biol. Chem.* **276**, 42801–42806.

14. Niu, S.-L., Mitchell, D. C. & Litman, B. J. (2001) *J. Biol. Chem.* **276**, 42807–42811.
15. Niu, S.-L., Mitchell, D. C. & Litman, B. J. (2002) *J. Biol. Chem.* **277**, 20139–20145.
16. Huber, T., Botelho, A. V., Beyer, K. & Brown, M. F. (2004) *Biophys. J.* **86**, 2078–2100.
17. Crozier, P. S., Stevens, M. J. & Woolf, T. B. (2003) *Biophys. J.* **84**, Suppl. S, 132A–132A.
18. Saam, J., Tajkhorshid, E., Hayashi, S. & Schulten, K. (2002) *Biophys. J.* **83**, 3097–3112.
19. Lemaitre, V., Yeagle, P. & Watts, A. (2005) *Biochemistry* **44**, 12667–12680.
20. Pitman, M. C., Grossfield, A., Suits, F. & Feller, S. E. (2005) *J. Am. Chem. Soc.* **127**, 4576–4577.
21. Feller, S. E., Gawrisch, K. & Woolf, T. B. (2003) *J. Am. Chem. Soc.* **125**, 4434–4435.
22. Stillwell, W. & Wassall, S. R. (2003) *Chem. Phys. Lipids* **126**, 1–27.
23. Brown, M. F. (1994) *Chem. Phys. Lipids* **73**, 159–180.
24. Farrens, D. L., Altenbach, C., Yang, K., Hubbell, W. L. & Khorana, H. G. (1996) *Science* **274**, 768–770.
25. Hubbell, W. L., Altenbach, C., Hubbell, C. M. & Khorana, H. G. (2003) *Adv. Protein Chem.* **63**, 243–290.
26. Berman, H. M., Westbrook, J., Feng, Z., Gilliland, G., Bhat, T. N., Weissig, H., Shindyalov, I. N. & Bourne, P. E. (2000) *Nucleic Acids Res.* **28**, 235–242.
27. Pitman, M. C., Suits, F., MacKerell, A. D., Jr., & Feller, S. E. (2004) *Biochemistry* **43**, 15318–15328.
28. Soubias, O. & Gawrisch, K. (2005) *J. Am. Chem. Soc.* **127**, 13110–13111.
29. Menkes, J. H., Alter, M., Steigleder, G. K., Weakely, D. & Sung, J. H. (1962) *Pediatrics* **29**, 764–779.
30. McLennan, P., Howee, P., Abeywardena, M., Muggli, R., Raederstorff, D., Mano, M., Rayner, T. & Head, R. (1996) *Eur. J. Pharmacol.* **300**, 83–89.
31. Bernsohn, J. & Stephanides, L. M. (1967) *Nature* **215**, 821–823.
32. Kremer, J. M., Lawrence, D. A., Jubiz, W., DiGiacomo, R., Rynes, R., Bartholomew, L. E. & Sherman, M. (1990) *Arthritis Rheum.* **33**, 810–820.
33. Das, U. N. (1994) *Prostaglandins Leukotrienes Essent. Fatty Acids* **51**, 207–213.
34. Pawlosky, R. J. & Salem, N., Jr. (1995) *Am. J. Clin. Nutr.* **61**, 1284–1289.
35. Hibbeln, J. R. & Salem, N., Jr. (1995) *Am. J. Clin. Nutr.* **62**, 1–9.
36. Laungharne, J. D., Mellor, J. E. & Pett, M. (1996) *Lipids* **31**, Suppl., 163–165.
37. Feller, S. E. & Gawrisch, K. (2005) *Curr. Opin. Struct. Biol.* **15**, 416–422.
38. Carrillo-Tripp, M. & Feller, S. E. (2005) *Biochemistry* **44**, 10164–10169.
39. Polozova, A. & Litman, B. J. (2000) *Biophys. J.* **79**, 2632–2643.
40. Albert, A. D., Young, J. E. & Yeagle, P. (1996) *Biochim. Biophys. Acta* **1285**, 47–55.
41. Wiedmann, T. S., Pates, R. D., Beach, J. M., Salmon, A. & Brown, M. F. (1988) *Biochemistry* **27**, 6469–6474.
42. MacKerell, A. D., Jr., Bashford, D., Bellott, M., Dunbrack, R., Jr., Evanseck, J., Field, M., Fischer, S., Gao, J., Guo, H., Ha, S., et al. (1998) *J. Phys. Chem. B* **102**, 3586–3616.
43. Klauda, J. B., Brooks, B. R., MacKerell, A. D., Jr., Venable, R. M. & Pastor, R. W. (2005) *J. Phys. Chem. B* **109**, 5300–5311.
44. Feller, S. E., Gawrisch, K. & MacKerell, A. D., Jr. (2002) *J. Am. Chem. Soc.* **124**, 318–326.
45. Brooks, B. R., Bruccoleri, R. E., Olafson, B. D., States, D. J., Swaminathan, S. & Karplus, M. (1983) *J. Comput. Chem.* **4**, 187–217.
46. Fitch, B. G., Germain, R. S., Mendell, M., Pitera, J., Pitman, M., Rayshubskiy, A., Sham, Y., Suits, F., Swope, W. C., Ward, T. J. C., et al. (2003) *J. Parallel Distrib. Comp.* **63**, 759–773.
47. Allen, F., Almasi, G., Andreoni, W., Beece, D., Berne, B. J., Bright, A., Brunheroto, J., Cascaval, C., Castanos, J., Coteus, P., et al. (2001) *IBM Syst. J.* **40**, 310–327.
48. Woolf, T. B. & Roux, B. (1996) *Proteins Struct. Funct. Genet.* **24**, 92–114.
49. Gaede, H. C. & Gawrisch, K. (2004) *Magn. Reson. Chem.* **42**, 115–122.